IEEE Access
Multidisciplinary ⋮ Rapid Review ⋮ Open Access Journal

Received 21 August 2023, accepted 8 September 2023, date of publication 13 September 2023, date of current version 20 September 2023.

Digital Object Identifier 10.1109/ACCESS.2023.3315118

RESEARCH ARTICLE

A Tanh Control Method for the Third Mirror's Z Axis of Large Optical Telescope

WENLIN ZHOU[1,2], KUN XIE[3], JUNZHANG QIAN[1,2], MO XIA[1,2], YI PU[1,2], JINLONG HUANG[1,2], AND XIN LI[1,2]

[1]Institute of Optics and Electronics, Chinese Academy of Sciences, Chengdu 610209, China
[2]National Key Laboratory of Optical Field Manipulation Science and Technology, Chinese Academy of Sciences, Chengdu 610209, China
[3]Xi'an Satellite Control Center, Xi'an 710043, China

Corresponding authors: Jinlong Huang (huangjl@ioe.ac.cn) and Xin Li (lixin@ioe.ac.cn)

This work was supported by the National Natural Science Foundation (NSFC) of China under Project 12293031.

ABSTRACT The position accuracy of the third mirror's Z axis will directly affect the measurement accuracy of the optical telescope, so it is necessary to improve the position accuracy. In order to improve the control performances of the third mirror's Z-axis of a large optical telescope, this paper proposes a novel control algorithm based on hyperbolic tangent function (tanh). The proposed algorithm is used to replace the traditional integral separated proportional-integral (IS-PI) controller which is widely used in industry servo control system. Firstly, a mathematical model of the third mirror's Z-axis is established. Secondly, a controller based on tanh is proposed, and the characteristics and stability of the algorithm are analyzed. Thirdly, the parameters tuning method of the proposed algorithm is given. The simulation results show that the proposed algorithm has higher tracking accuracy than IS-PI controller. Finally, experiments are carried out on a large optical telescope's Z axis. In the experiments, IS-PI controller and tanh controller are compared, and the results show that the control performances are greatly improved.

INDEX TERMS High precision position control, motor control, hyperbolic tangent function, optical telescope, integral separation proportional integral.

I. INTRODUCTION

Large optical telescope is a kind of high-precision equipment for astronomical observation. Important scientific achievements in astronomy and astrophysics rely heavily on the observation data of optical telescopes [1], [2], [3]. The optical structure of a large optical telescope mainly includes primary mirror, secondary mirror and third mirror. The main function of the third mirror is optical path refraction, which refracts the beam from the secondary mirror to Cassgrain focus, folding axis focus, Coude focus, etc. As an observation instrument, the observing efficiency of a telescope is one of the key performance parameters. So, it is necessary to make full use of the focus point to make the telescope have multi-focus capabilities. The third mirror, which can be freely switched, is a key component for changing focus and improving the observing efficiency of the telescope, and it is getting more and more attention [4].

Usually, optical telescopes operate within the visible and infrared wavelength range of electromagnetic waves, therefore, there are extremely high requirements for the accuracy of optical systems. The rotation and repeated positioning accuracy of the third mirror directly affects the pointing accuracy of the optical telescope [5]. And when the control performances are not good enough, it will lead to a significant decrease in the optical performance of the telescope. The third mirror's Z-axis control needs to achieve two goals: 1) fast switching. 2) high position accuracy.

In order to achieve high-performance control goals, nonlinear PID controller, fuzzy controller, sliding mode controller, active disturbance rejection controller (ADRC) [6], [7], [8], [9], [10], [11], are studied and good control performances have been achieved. However, at present, the most commonly used control method in control engineering is still

The associate editor coordinating the review of this manuscript and approving it for publication was Md. Selim Habib.

proportional-integral-differential (PID) controller [12], [13]. Although many control methods based on PID are often used in engineering, how to turning the parameters to achieve the best control performance is still being studied [14]. To solve the PID parameter tuning problem, Lawrence N P [15] and Dogru O [16] use deep learning for PID parameter tuning. CHAI Tian-You [17] proposed a PID tuning intelligent system based on end-edge-cloud collaboration. It is a good idea to study how to adjust PID parameters to optimize control performance. In addition, we can also study a controller that has similar control performance to PID controllers, but with easier parameter turning.

The hyperbolic function is a very common function that is widely studied and used in neural networks, filters [18], tracking differentiators [19], etc. Zhang proposed a fuzzy hyperbolic model (FHM) based on hyperbolic tangent [20], [21], [22], [23], [24], and the analysis showed that the control algorithm has very strong nonlinearity coping ability. However, using the hyperbolic tangent function as a controller has not been studied and used in application. In this paper, we propose a control algorithm based on hyperbolic tangent function to improve the control performances of the third mirror's Z axis. The proposed algorithm is an error-based controller and does not need an accurate model of the plant. Since differential will amplify the sensor noise, PI control is often used in motor control engineering [25], [26]. At present, the most commonly used control method in optical telescopes is integral separation proportional integral (IS-PI) algorithm [27], which is a fundamental form of nonlinear PI control algorithm. This control algorithm can be added in traditional three closed-loop control architecture to replace the IS-PI based position controller. The similarity and differences between the proposed controller and PI controller can be seen by the Laplace transform [28], [29], [30], [31], which is similar to a variable-gain PI control algorithm. In order to verify the control performance of the controller proposed in this paper, we will compare it with the IS-PI controller through simulation and experimentation.

This paper is organized as follows: In section II, the simplified mathematical model of the third mirror's Z axis for large optical telescope is introduced. In section III, a tanh algorithm is proposed, and the stability and simulation result are analyzed. Section IV provides the experimental results, and compared with the integral separation control algorithm. The summary is drawn in Section V.

II. MECHANICAL STRUCTURE AND MATHEMATICAL MODEL OF THE THIRD MIRROR's Z AXIS FOR LARGE TELESCOPE

A. MECHANICAL STRUCTURE

The optical telescope is traditional alt-azimuth structure, as shown in Fig.1. And the third mirror's Z axis is a key mechanism of the telescope, which is used to achieve high-precision and rapid switching between different terminals focus.

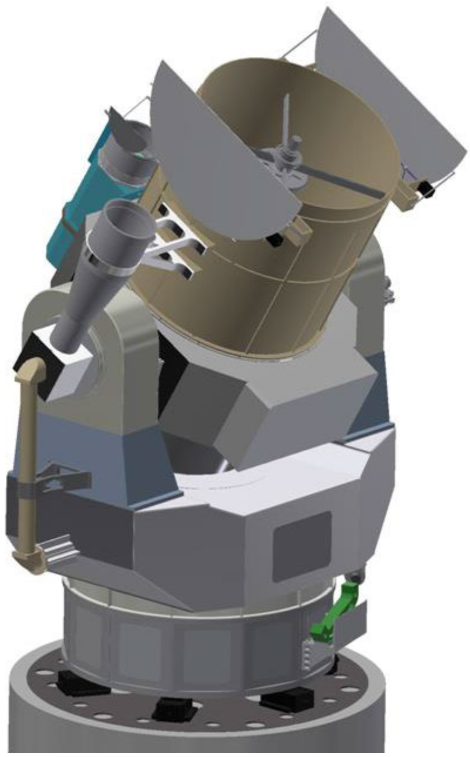

FIGURE 1. The structure of a large optical telescope.

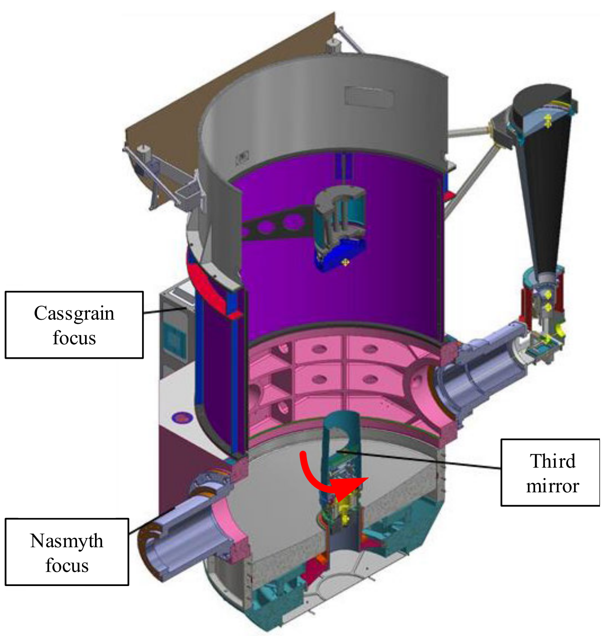

FIGURE 2. Schematic diagram of the third mirror rotation.

Fig.2 is the schematic diagram of the Z-axis rotation of the third mirror. Fig.3 is the physical picture of the rotating axis mechanism of the third mirror (the third mirror is not installed).

Fig.4 shows the mechanical structure of the rotating shaft of the third mirror's Z-axis. The Z axis is equipped with

FIGURE 3. Physical object of the third mirror's Z-axis mechanism.

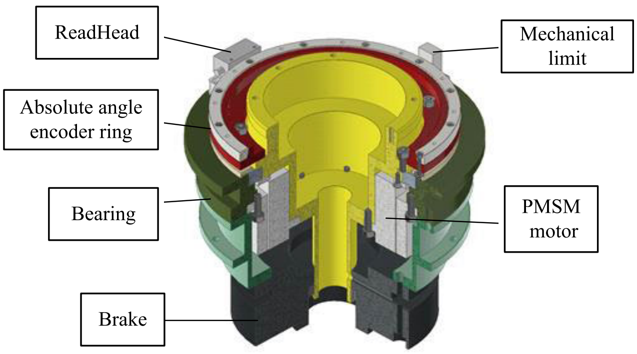

FIGURE 4. Composition of the third mirror's Z-axis mechanism.

a permanent magnet synchronous motor (PMSM) and a high-precision position sensor. One brake is installed on the shafting to provide braking torque when the system is not powered on.

B. MATHEMATICAL MODEL OF THE THIRD MIRROR's Z AXIS FOR LARGE TELESCOPE

For simplicity, a simplified model of the third mirror's Z axis system is as shown in Fig.5. The model consists of a series of mass-spring systems, with a motor and a position sensor. The load inertia is J_L, the motor inertia is J_M, the stiffness is K_s, the corresponding viscosity is b_s. T_M is the torque provided by the motor. θ_M, ω_M, a_M and θ_L, ω_L, a_L are the position, velocity, and acceleration of each inertia respectively. T_d is the disturbance torque, including unbalance torque, etc. T_f is the friction torque. c_f and c_v are the Coulomb coefficient and viscous coefficient.

Usually, the bandwidth of the current loop of PMSM is high. So the mathematical model of PMSM [11] can be regarded as:

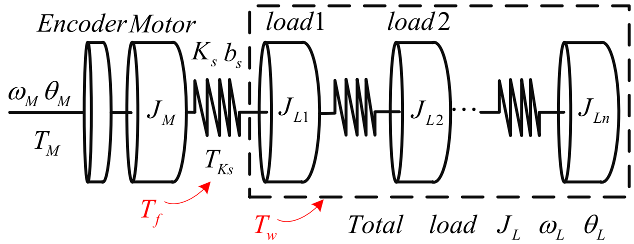

FIGURE 5. Simplified model of the third mirror's Z axis system.

$$T_M = I_M \cdot [k_T + k_M \sin(n \cdot \theta_M + \varphi_M)] \tag{1}$$

where I_M is the I_q current of the motor, k_T is the nominal torque coefficient of the motor, $k_M \sin(n \cdot \theta_M + \varphi_M)$ is used to simulate the torque fluctuation. The inputs of motor system are $u = I_M$. The state variables are selected as $x = \left[\theta_M\ \theta_L\ \omega_M\ \omega_L\right]^T$, among which θ_L and ω_L are unmeasurable. The output variables are selected as $y = \left[\theta_M\ \theta_L\right]^T$. So the corresponding state space equations of the model are:

$$\begin{cases} \dot{\theta}_M = \omega_M \\ \dot{\theta}_L = \omega_L \\ \dot{\omega}_M = -\frac{K_s}{J_M} \cdot \theta_M + \frac{K_s}{J_M} \cdot \theta_L - \frac{b_s}{J_M} \cdot \omega_M + \frac{b_s}{J_M} \cdot \omega_L \\ -\frac{c_v}{J_M} \cdot \omega_M - sign\left(\dot{\theta}_M\right) \cdot \frac{c_f}{J_M} \\ +\frac{k_T + k_M \sin(n \cdot \theta_M + \varphi_M)}{J_M} \cdot I_M \\ \dot{\omega}_L = \frac{K_s}{J_L} \cdot \theta_M - \frac{K_s}{J_L} \cdot \theta_L + \frac{b_s}{J_L} \cdot \omega_M - \frac{b_s}{J_L} \cdot \omega_L - \frac{1}{J_L} \cdot T_d \end{cases} \tag{2}$$

And the goal of the control system is that: for a given reference θ_{ref} and under unknown disturbances $\theta_M \to \theta_{ref}$.

III. DERIVATION OF TANH ALGORITHM

A. TANH ALGORITHM FRAMEWORK

As we all know, $\tanh(x) = \frac{e^x - e^{-x}}{e^x + e^{-x}}$, and its first and second derivative of the function are shown in Fig.6.

From Fig.6, we can see that $\tanh(x)$ and its first and second derivatives are smooth and bounded. It has the following properties:

$$\tanh(x) \approx \begin{cases} 1, & x > 5 \\ x, & -0.3 < x < 0.3 \\ -1, & x < -5 \end{cases} \tag{3}$$

When $0.3 < x < 5$ or $-5 < x < -0.3$, the output of $\tanh(x)$ is nonlinear. From Fig.6, we can see that if hyperbolic tangent function is used as the position loop controller, the output of the controller is smooth. Based on the hyperbolic tangent function, we build the tanh controller, whose expression is as follows:

$$f(x) = k \tanh(a \cdot x) = k \frac{e^{a \cdot x} - e^{-a \cdot x}}{e^{a \cdot x} + e^{-a \cdot x}} \tag{4}$$

where $k > 0$, $a > 0$ are tunable parameters and x is input position error. $e = 2.71828$ is the natural logarithm.

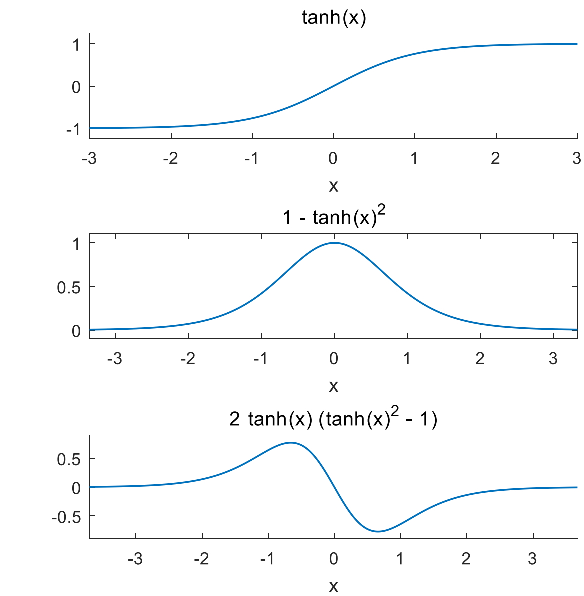

FIGURE 6. tanh(x) function and its derivatives.

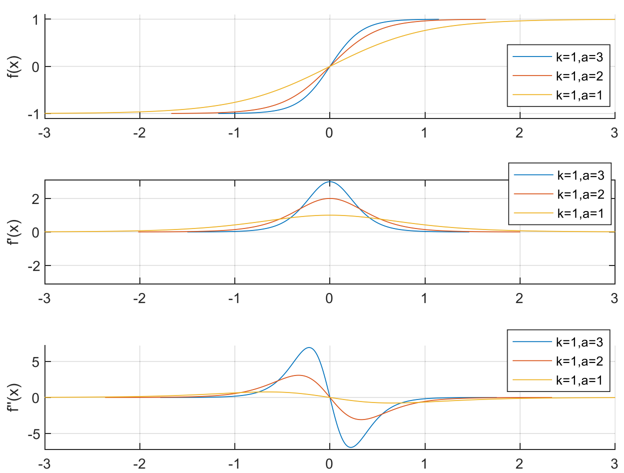

FIGURE 7. $k \tanh(a \cdot x)$, $k = 1$, a takes different values.

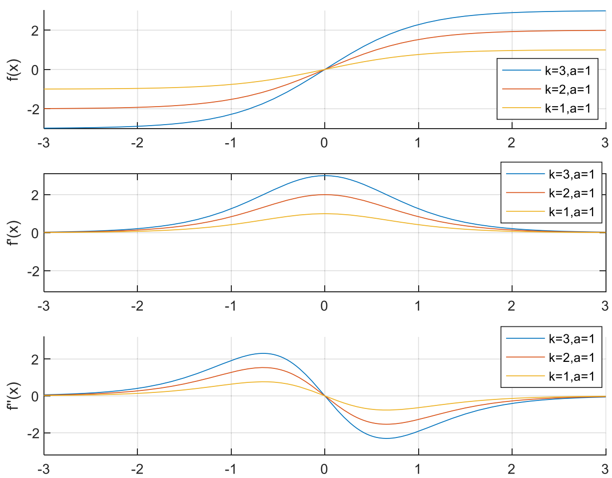

FIGURE 8. $k \tanh(a \cdot x)$, $a = 1$, k takes different values.

When k and a takes different values, the output of the function is shown in Fig.7 and Fig.8, it can be seen that the max value of $k \tanh(a \cdot x)$ is determined by k. The slope of $k \tanh(a \cdot x)$ is determined by k and a. It can be seen that both the first and second derivatives of $f(x)$ are bounded and smooth.

In order to further analyze the characteristics of equation (4), the Laplace transform is performed as follow [28], [29], [30]:

$$\begin{aligned}\mathcal{L}[k \tanh(at)](s) &= \int_0^\infty e^{-st} k \tanh(at)\, dt \\ &= \frac{k}{2a} \cdot \frac{\psi^{(0)}\left(\frac{a}{4s}+\frac{1}{2}\right) - s\psi^{(0)}\left(\frac{s}{4a}\right) - 2a}{s}\end{aligned} \tag{5}$$

In which $\psi^{(0)}(z) = \frac{\Gamma'(z)}{\Gamma(z)}$, $\Gamma(z) = \int_0^\infty e^{-t} t^{z-1} dt$.

If $x > 0$, the Digamma function is defined as the first derivative of the logarithm of the gamma function, with the following integrals or series representation [28], [29], [30], [31]:

$$\begin{aligned}\psi^{(0)}(x) &= -\gamma + \int_0^\infty \frac{e^{-t} - e^{-xt}}{1-e^{-t}} dt \\ &= -\gamma - \frac{1}{x} + \sum_{n=1}^{\infty} \frac{x}{n(n+x)}\end{aligned} \tag{6}$$

In which $\gamma = 0.57721$ is Euler constant.

Because $k > 0$ and $a > 0$, we have: $A = \left(\frac{a}{4s}+\frac{1}{2}\right) = \frac{2s+a}{4s} > 0$ and $B = \frac{s}{4a} > 0$, it can be obtained by using (5), (6), and (7), as shown at the bottom of the next page.

A traditional PI controller is:

$$G_{pi}(s) = k_p + \frac{k_i}{s} \tag{8}$$

Compared (7) and (8), we can see that tanh controller is similar to PI controller, but the difference is that it is a variable-gain controller. From Fig.6 we know that the smaller the input error x, the greater the controller gain. This reduces the overshoot with small gain when the error is large. At small errors, large gains can reduce steady-state errors.

B. TANH CONTROLLER DESIGN

Fig.9 is the block diagram of Tanh controller, Tanh control method is used as a position controller. The controller is as follows:

$$\omega_{ref} = \omega_{\max} \tanh(k_\omega e_\theta) = \omega_{\max} \frac{e^{k_\omega e_\theta} - e^{-k_\omega e_\theta}}{e^{k_\omega e_\theta} + e^{-k_\omega e_\theta}} \tag{9}$$

ω_{ref} is the reference speed value of the position closed-loop output, ω_{max} is the maximum speed of the motor, k_ω is the tuning parameter and $k_\omega > 0$, θ_{ref} is the desired position, θ_M is the motor's actual position, $e_\theta = \theta_{ref} - \theta_M$ is the position error, $e = 2.71828$ is the natural logarithm, according to (4), we can get $-\omega_{\max} \le \omega_{ref} \le \omega_{\max}$.

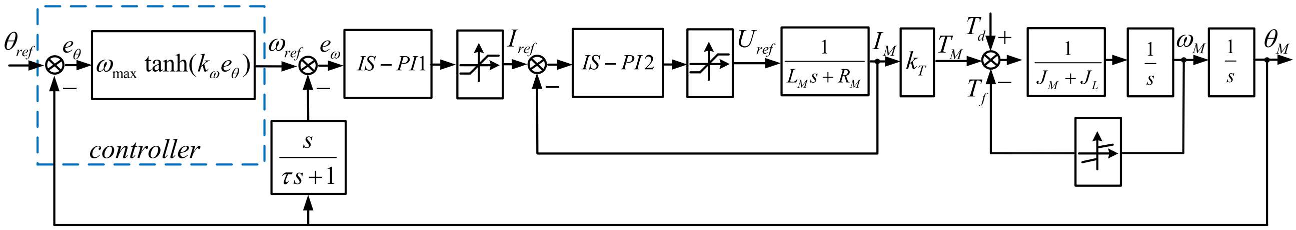

FIGURE 9. Tanh control block diagram.

The discretization form of (9) is:

$$\omega_{ref}(k) = \omega_{\max}\tanh(k_\omega e_\theta(k)) \tag{10}$$

IS-PI controller is used for speed closed-loop control:

$$e_\omega = \omega_{ref} - \omega_M$$
$$I_M = \begin{cases} k_p \cdot e_\omega + k_i \cdot \int_0^t e_\omega dt,\ e_\omega \le e_0 \\ sgn(e_\omega)\, c\sqrt{e_\omega}, \quad e_\omega > e_0 \end{cases} \tag{11}$$

In which $sgn(e_\omega) = \begin{cases} 1,\ e_\omega > 0 \\ -1,\ e_\omega < 0 \end{cases}$ is the sign of input error. c, k_p and k_i are turning parameters. The value of e_0 is determined by c, k_p and k_i, we must ensure that when the value of e_ω is different, the output of I_M is smooth. When the parameter $c = 0$, let $e_0 > e_{max}$, the IS-PI controller become a PI controller.

The discretization form of (11) is:

$$I_M(k) = \begin{cases} k_p \cdot e_\omega(k) + k_i \cdot (e_\omega(k) + e_\omega(k-1)) \\ +I_M(k-1),\ e_\omega \le e_0 \\ sgn(e_\omega(k))\, c\sqrt{e_\omega(k)},\ e_\omega > e_0 \end{cases} \tag{12}$$

In order to protect the motor and the drive system, the output of the speed controller is limited by the saturation, so:

$$I_{out}(k) = \begin{cases} I_{\max},\ I_M(k) \ge I_{\max} \\ I_M(k),\ -I_{\max} < I_M(k) < I_{\max} \\ -I_{\max},\ I_M(k) \le -I_{\max} \end{cases} \tag{13}$$

where $I_{\max}$ is the maximum current, $I_{out}(k)$ is the output of the speed controller.

C. STABILITY ANALYSIS

By discretizing (2), we can get:

$$\begin{cases} \theta_M(k+1) = \omega_M(k) \cdot T + \theta_M(k) \\ \theta_L(k+1) = \omega_L(k) \cdot T + \theta_L(k) \\ \omega_M(k+1) = \omega_M(k) - \frac{K_s}{J_M} \cdot \theta_M(k) \cdot T + \frac{K_s}{J_M} \cdot \theta_L(k) \cdot T - \\ \frac{b_s}{J_M} \cdot \omega_M(k) \cdot T + \frac{b_s}{J_M} \cdot \omega_L(k) \cdot T - \\ \frac{c_v}{J_M} \cdot \omega_M(k) \cdot T - sign(\omega_M(k)) \cdot \frac{c_f}{J_M} \cdot T \\ + \frac{k_T + k_M \sin(n \cdot \theta_M(k) + \varphi_M(k))}{J_M} \cdot I_{out}(k) \cdot T \\ \omega_L(k+1) = \frac{K_s}{J_L} \cdot \theta_M(k) \cdot T - \frac{K_s}{J_L} \cdot \theta_L(k) \cdot T + \\ \frac{b_s}{J_L} \cdot \omega_M(k) \cdot T - \frac{b_s}{J_L} \cdot \omega_L(k) \cdot T - \\ \frac{1}{J_L} \cdot T_d(k) \cdot T + \omega_L(k) \end{cases} \tag{14}$$

where T is the sampling period.

Since cascade control is used, the stability of the inner loop controller is first demonstrated.

1) THE STABILITY OF VELOCITY CLOSED-LOOP CONTROLLER

Let:

$$e_\omega(k+1) = \omega_{ref} - \omega_M(k+1) \tag{15}$$
$$e_\omega(k) = \omega_{ref} - \omega_M(k) \tag{16}$$

The Lyapunov function is designed as [25]:

$$V(k) = \frac{1}{2}e_\omega^2(k) \tag{17}$$

We can get $\forall \omega_{ref}(k) \ne \omega_M(k)$, $V(k) > 0$.

$$\begin{aligned} \mathcal{L}[k\tanh(at)](s) &= \frac{k}{2a}\frac{-\gamma - \frac{1}{A} + \sum_{n=1}^{\infty}\frac{A}{n(n+A)} - s\left(-\gamma - \frac{1}{B} + \sum_{n=1}^{\infty}\frac{B}{n(n+B)}\right) - 2a}{s} \\ &= \frac{k}{2a}\frac{-\gamma - \frac{1}{\frac{2s+a}{4s}} + \sum_{n=1}^{\infty}\frac{\frac{2s+a}{4s}}{n\left(n+\frac{2s+a}{4s}\right)} - s\left(-\gamma - \frac{1}{\frac{s}{4a}} + \sum_{n=1}^{\infty}\frac{\frac{s}{4a}}{n\left(n+\frac{s}{4a}\right)}\right) - 2a}{s} \\ &= \frac{k}{2a}\left[\gamma + \frac{(2a-\gamma)}{s}\right] - \frac{2ks}{a(2s+a)} + \frac{k}{2a}\sum_{n=1}^{\infty}\frac{2s+a}{ns(4ns+2s+a)} \\ &\quad - \frac{k}{2a}\sum_{n=1}^{\infty}\frac{s}{n(s+4an)} \end{aligned} \tag{7}$$

According (14), (15), (16) and (17), we have:

$$\begin{aligned}
\Delta V(k) &= V(k+1) - V(k) \\
&= \frac{1}{2}e_{\omega}^{2}(k+1) - \frac{1}{2}e_{\omega}^{2}(k) \\
&= \frac{1}{2}\left(\omega_{ref} - \omega_M(k+1)\right)^2 - \frac{1}{2}\left(\omega_{ref} - \omega_M(k)\right)^2 \\
&= \frac{1}{2}\left(\omega_{ref} - (\delta + \omega_M(k))\right)^2 - \frac{1}{2}\left(\omega_{ref} - \omega_M(k)\right)^2 \\
&= \frac{1}{2}\left(\omega_{ref} - \omega_M(k)\right)^2 \cdot \left(1 - \frac{\delta}{\omega_{ref} - \omega_M(k)}\right)^2 \\
&\quad - \frac{1}{2}\left(\omega_{ref} - \omega_M(k)\right)^2 \\
&= \frac{1}{2}\left(\omega_{ref} - \omega_M(k)\right)^2 \\
&\quad \cdot \left(-\frac{2\delta}{\omega_{ref} - \omega_M(k)} + \left(\frac{\delta}{\omega_{ref} - \omega_M(k)}\right)^2\right)
\end{aligned} \tag{18}$$

In which:

$$\begin{aligned}
\delta &= -\frac{K_s}{J_M}\cdot\theta_M(k)\cdot T + \frac{K_s}{J_M}\cdot\theta_L(k) \\
&\quad \cdot T - \frac{b_s}{J_M}\cdot\omega_M(k)\cdot T \\
&\quad + \frac{b_s}{J_M}\cdot\omega_L(k) \\
&\quad \cdot T - \frac{c_v}{J_M}\cdot\omega_M(k)\cdot T - sign(\omega_M(k))\cdot\frac{c_f}{J_M}\cdot T \\
&\quad + \frac{k_T + k_M\sin(n\cdot\theta_M(k) + \varphi_M(k))}{J_M} \\
&\quad \cdot I_{out}(k)\cdot T
\end{aligned} \tag{19}$$

If $\Delta V(k) < 0$, velocity error $e_{\omega}(k)$ is asymptotically convergent, we have $\omega_M \to \omega_{ref}$. So we need:

$$\begin{aligned}
\Delta V(k) &= \\
&\frac{1}{2}\left(\omega_{ref} - \omega_M(k)\right)^2 \\
&\quad \cdot \left(-\frac{2\delta}{\omega_{ref} - \omega_M(k)} + \left(\frac{\delta}{\omega_{ref} - \omega_M(k)}\right)^2\right) < 0
\end{aligned} \tag{20}$$

Let $\rho = \frac{\delta}{\omega_{ref} - \omega_M(k)}$, so when $0 < \rho < 2$, $\Delta V(k) < 0$. According (19) we have:

$$\begin{aligned}
\rho &= \frac{\delta}{e_{\omega}(k)} \\
&= -\frac{K_s}{J_M e_{\omega}(k)}\cdot\theta_M(k)\cdot T + \frac{K_s}{J_M e_{\omega}(k)}\cdot\theta_L(k)\cdot T \\
&\quad - \frac{b_s}{J_M e_{\omega}(k)}\cdot\omega_M(k)\cdot T + \frac{b_s}{J_M e_{\omega}(k)}\cdot\omega_L(k)\cdot T \\
&\quad - \frac{c_v}{J_M e_{\omega}(k)}\cdot\omega_M(k)\cdot T - sign(\omega_M(k))\cdot\frac{c_f}{J_M e_{\omega}(k)}\cdot T \\
&\quad + \frac{k_T + k_M\sin(n\cdot\theta_M(k) + \varphi_M(k))}{J_M e_{\omega}(k)}\cdot I_{out}(k)\cdot T
\end{aligned} \tag{21}$$

Further, according to equations (12):

$$\begin{aligned}
\rho &= -\frac{K_s}{J_M e_{\omega}(k)}\cdot\theta_M(k)\cdot T + \frac{K_s}{J_M e_{\omega}(k)}\cdot\theta_L(k)\cdot T \\
&\quad - \frac{b_s}{J_M e_{\omega}(k)}\cdot\omega_M(k)\cdot T + \frac{b_s}{J_M e_{\omega}(k)}\cdot\omega_L(k)\cdot T \\
&\quad - \frac{c_v}{J_M e_{\omega}(k)}\cdot\omega_M(k)\cdot T - sign(\omega_M(k))\cdot\frac{c_f}{J_M e_{\omega}(k)}\cdot T \\
&\quad + \frac{k_T + k_M\sin(n\cdot\theta_M(k) + \varphi_M(k))}{J_M e_{\omega}(k)} I_{out}(k)\cdot T \\
&= A - B
\end{aligned} \tag{22}$$

In which:

$$A = \frac{(k_T + k_M\sin(n\cdot\theta_M(k) + \varphi_M(k)))}{J_M e_{\omega}(k)}\cdot I_{out}(k)\cdot T \tag{23}$$

and

$$\begin{aligned}
B &= \frac{K_s(\theta_M(k) - \theta_L(k)) + b_s(\omega_M(k) - \omega_L(k))}{J_M e_{\omega}(k)}\cdot \\
&\quad T + \frac{c_v\omega_M(k) + sign(\omega_M(k))\, c_f}{J_M e_{\omega}(k)}\cdot T
\end{aligned} \tag{24}$$

Ignoring motor torque fluctuations, (23) can be simplified to:

$$A = \begin{cases} \frac{k_T\left(k_p\cdot e_{\omega}(k) + k_i\cdot(e_{\omega}(k) + e_{\omega}(k-1)) + I_M(k-1)\right)}{J_M e_{\omega}(k)}\cdot T, & e_{\omega} \le e_0 \\ \frac{k_T\left(sgn(e_{\omega}(k))c\sqrt{e_{\omega}(k)}\right)}{J_M e_{\omega}(k)}\cdot T, & e_{\omega} > e_0 \end{cases} \tag{25}$$

Commonly, we have $\theta_M(k) - \theta_L(k) \ll \varepsilon$, $\omega_M(k) - \omega_L(k) << \varepsilon$, $\varepsilon \to 0$. Ignoring these two items, (24) can be simplified to:

$$B = \frac{c_v\omega_M(k) + sign(\omega_M(k))\, c_f}{J_M e_{\omega}(k)}\cdot T \tag{26}$$

According (25) and (26), we can find the appropriate parameters $c > 0$, $k_p > 0$ and $k_i > 0$ to make $A > B$ and $A < 2 + B$, at this time $0 < \rho < 2$, $\Delta V(k) < 0$ can be satisfied. At the same time, it can be seen that the smaller the sampling time T, the easier it is to meet this condition. Thus, the error of speed closed-loop controller is asymptotically convergent. From the above theoretical analysis, we can see that the stability of the velocity closed-loop system can be guaranteed.

2) THE STABILITY OF POSITION CLOSED-LOOP CONTROLLER

When the speed closed-loop control is stable, with $\omega_M \to \omega_{ref}$, we can assume $\omega_M = \omega_{ref}$, so we can see from (10) :

$$\omega_{ref} = \omega_{\max}\tanh\left(k_{\omega}\left(\theta_{ref} - \theta_M\right)\right) \tag{27}$$

The Lyapunov function is designed as follows:

$$V(t) = \ln\left(\cosh\left(k_{\omega}\left(\theta_{ref} - \theta_M\right)\right)\right) \tag{28}$$

Because $\cosh(x) = \frac{e^x+e^{-x}}{2} \geq (e^x)^{\frac{1}{2}}(e^{-x})^{\frac{1}{2}} = 1$, $\cosh\left(k_\omega\left(\theta_{ref}-\theta_M\right)\right) \geq 1$, we can get $\forall\theta_{ref} \neq \theta_M$, $V(t) > 0$, It can be obtained that:

$$\begin{aligned}
&\dot{V}(t) \\
&= \tanh\left(k_\omega\left(\theta_{ref}-\theta_M\right)\right) \cdot k_\omega \cdot \left(-\dot{\theta}_M\right) \\
&= -k_\omega \tanh\left(k_\omega\left(\theta_{ref}-\theta_M\right)\right) \cdot \omega_{\max} \tanh\left(k_\omega\left(\theta_{ref}-\theta_M\right)\right) \\
&= -k_\omega\omega_{\max}\left(\tanh\left(k_\omega\left(\theta_{ref}-\theta_M\right)\right)\right)^2 \qquad (29)
\end{aligned}$$

Because $\omega_{\max} > 0$, When $k_\omega > 0$, $\dot{V}(t) < 0$. So the stability of the position closed-loop system can be guaranteed.

D. PARAMETER TUNING METHOD

The proposed algorithm only have 2 parameters: k_ω, $\omega_{\max}$. $\omega_{\max}$ do not need to be tuned, $\omega_{\max}$ is the maximum velocity of the system. How to adjust the parameter k_ω will be derived below.

According (10), we know when the position error $e_\theta(k) \leq e_\Delta$, the speed will begin to decrease. In order to ensure the smooth of the output speed under different position error $e_\theta(k)$, we have:

$$\omega_{\max}\tanh\left(k_\omega e_\Delta\right) = \omega_{\max} \qquad (30)$$

According (3) we have $\tanh(5) = 1$, so the value of k_ω is according to the e_Δ.

$$k_\omega = \frac{5}{e_\Delta} \qquad (31)$$

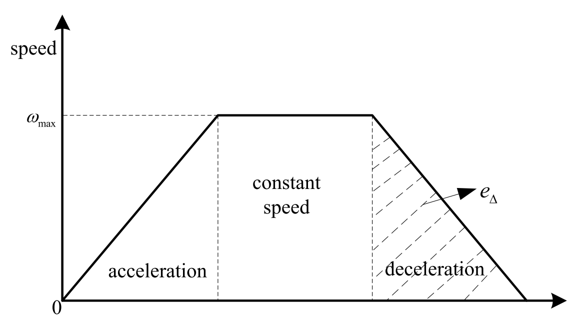

FIGURE 10. Uniform acceleration and deceleration.

As shown in Fig.10 we can derive e_Δ by the uniform acceleration and deceleration method:

$$e_\Delta \approx \frac{\omega_{\max}^2}{2a_{\max}} \qquad (32)$$

In which $a_{\max}$ is the maximum acceleration. So we have:

$$k_\omega \approx \frac{10a_{\max}}{{\omega_{\max}}^2} \qquad (33)$$

k_ω is adjusted according to the maximum acceleration and maximum velocity. Therefore, we can calculate the value of the tuning parameters through actual requirements and do not need to identify the accurate model of the control object, which is more convenient for engineers than IS-PI control.

TABLE 1. Position error comparision.

Tracking signal	Control method position tracking error			
	IS-PI		Tanh	
	PV	RMS	PV	RMS
$y = 2^\circ\sin(0.5t)$	$18.48''$	$0.33''$	$6.36''$	$0.11''$
$y = 2^\circ\sin(t)$	$24.55''$	$0.86''$	$11.42''$	$0.33''$
$y = 5^\circ\sin(t)$	$31.03''$	$1.85''$	$10.21''$	$0.54''$

PV stands for peak to peak value, RMS stands for root mean square. The unit is arc-second.

E. SIMULATION RESULTS

Due to the lack of integral separation in traditional PI control, there is significant overshoot, which can cause significant oscillations. In the simulation, Integral separation proportional integral (IS-PI) controller and tanh controller are tested respectively. Simulation model is shown in Fig.11. In order to reduce the tracking error, combined with speed feedforward. Since the maximum speed and current output of the motor are limited, there is a saturation link behind each IS-PI controller, which protects the motor and motor driver. The controller is the controller to be compared, and the other parts are exactly the same.

The common parameters of speed closed-loop(IS-PI1) are the same: $k_p = 0.175$, $k_i = 20$, $I_{\max} = 10$, $c = 0$. The common parameters of current closed-loop(IS-PI2) are the same: $k_p = 31.4159$, $k_i = 1200$, $c = 0$, these parameters are determined by the motor's inductance and resistance. The IS-PI controller parameters of position closed-loop are $k_p = 100$, $k_i = 0.01$, $\omega_{\max} = 250$, $c = 65$, $e_0 = 0.05^\circ$. The tanh control parameters of position closed-loop are $\omega_{\max} = 250$, $k_\omega = 1.05$. The coulomb friction coefficient is $c_f = 0.05$ and the viscous friction coefficient is $c_v = 0.05$. The sampling time is $T = 0.0001s$.

1) A COMPARISON OF STEP SIGNAL TRACKING SIMULATION

The step response is shown in Fig.12.

From Fig.12, we can see that settling time and overshoot of tanh controller is smaller than IS-PI controller. What's more, steady-state error of the tanh controller is $0.58''$, while for the IS-PI controller is $0.99''$.

2) A COMPARISON OF SINE SIGNAL TRACKING SIMULATION

The tracking errors of different sine signals are shown in Fig. 13, Fig. 14, Fig. 15 and table 1.

When reference signal is $2^\circ\sin(0.5t)$, the maximum speed of tracking signal is $1^\circ/s$, the results are shown in Fig.13, and table 1. When reference signal is $2^\circ\sin(t)$, the maximum speed of tracking signal is $2^\circ/s$, the results are shown in Fig.14, and table 1. When reference signal is $5^\circ\sin(t)$, the maximum speed of tracking signal is $5^\circ/s$, the results are shown in Fig.15, and table 1.From Fig. 13, Fig. 14, Fig. 15 and table 1, we can see that the tracking error RMS value and PV value of tanh control algorithm are smaller than those of IS-PI control algorithm.

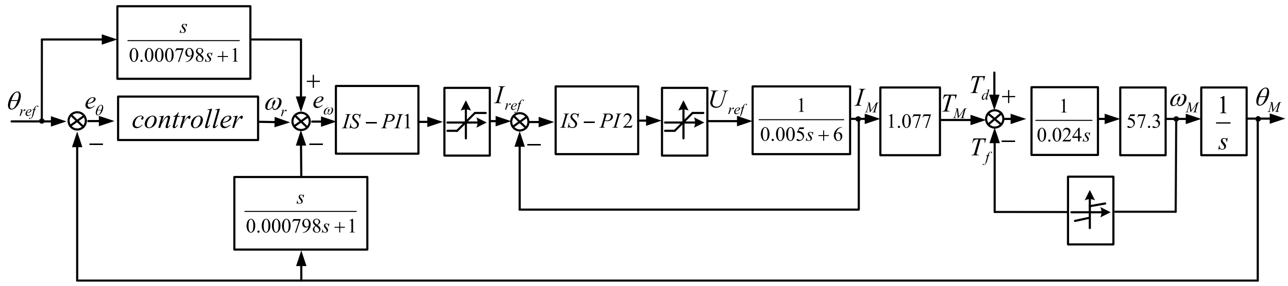

FIGURE 11. Block diagram of Simulation.

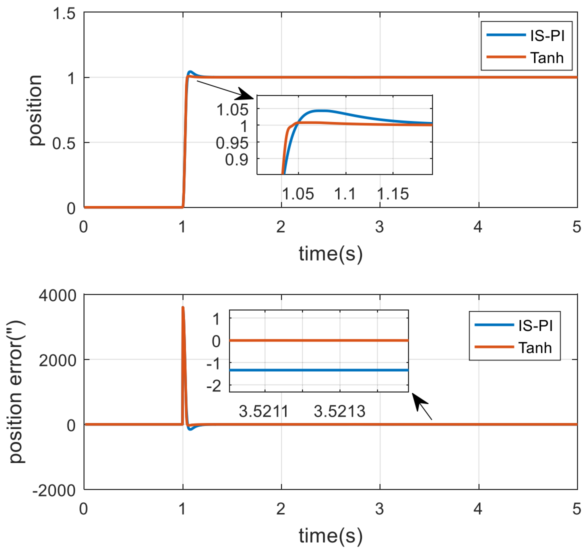

FIGURE 12. Step signal tracking simulation results.

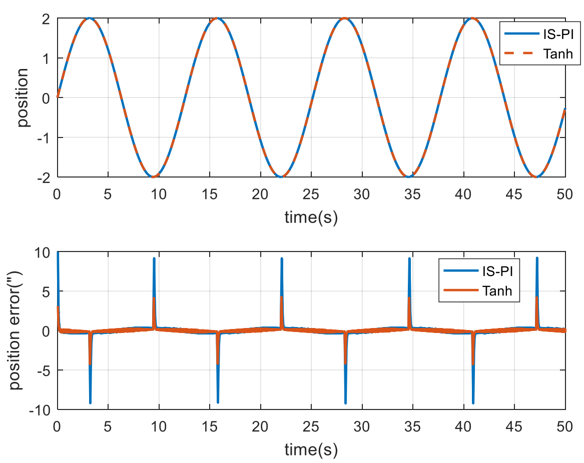

FIGURE 13. Sine signal 2° sin(0.5t) tracking simulation results.

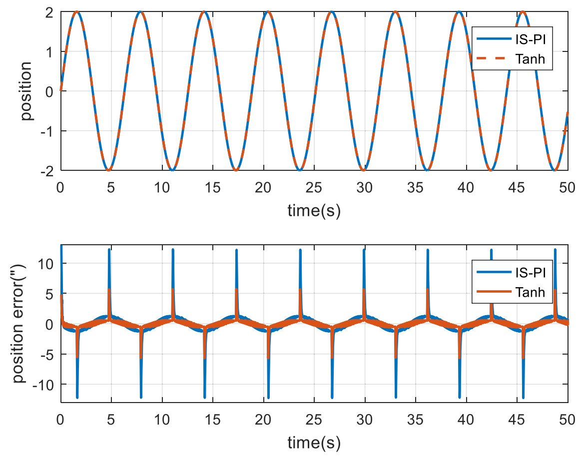

FIGURE 14. Sine signal 2° sin(t) tracking simulation results.

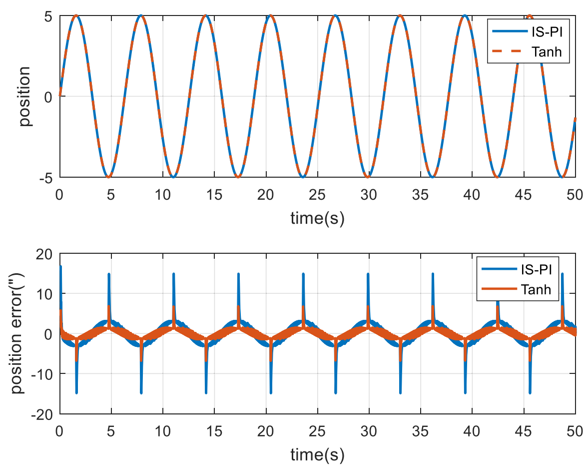

FIGURE 15. Sine signal 5° sin(t) tracking simulation results.

From the simulation results, it can be seen that the method proposed in this paper effectively reduces the peaks in the position errors. Compared with IS-PI controller, the tracking error PV (peak-to-peak) value is reduced by nearly 53.5%.

IV. EXPERIMENTS

A. EXPERIMENT AND PARAMETERS SETUP

The experimental setup is shown in Fig.16. The isolated power and control unit are installed inside the box on the telescope mount. The control unit is a DSP TMS320F28379D based board, which completes the encoder data acquisition, position loop, speed loop and current loop calculation. The operation frequency of speed and position loop is 1kHz, and the current loop is 16kHz. The current loop adopts the field oriented control (FOC) algorithm based on IS-PI controller, and the bandwidth of the current closed-loop is 800Hz. A high precision position sensor is installed at ends of the Z axis, and the resolution is 32 bits. The data recorded by the host computer and the recording frequency of is 100Hz. The parameters of the system are shown in table 2.

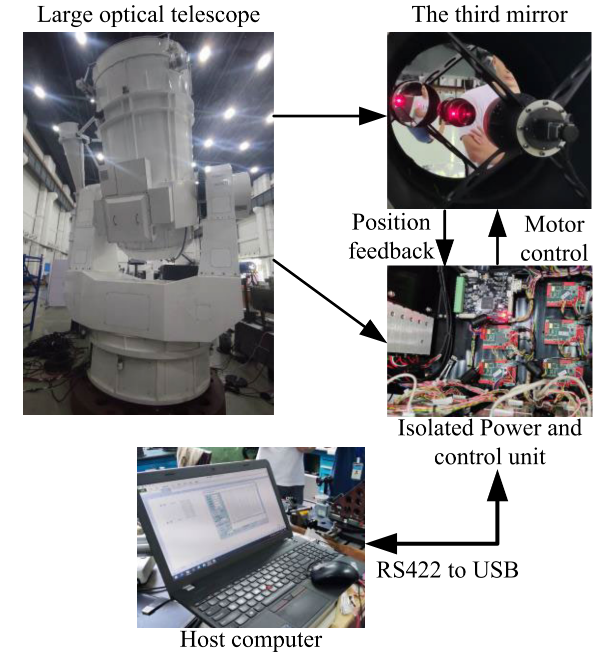

FIGURE 16. Experiment setup.

TABLE 2. Known parameters of the system.

Symbol	Quantity	Values
I_N	Nominal current of I_q	$4A$
J_m	Motor inertia	$0.0004kg \cdot m^2$
J_L	Load inertiar	$0.018kg \cdot m^2$
P_n	Pole number	24
k_M	Torque ripple coefficient	4.7%

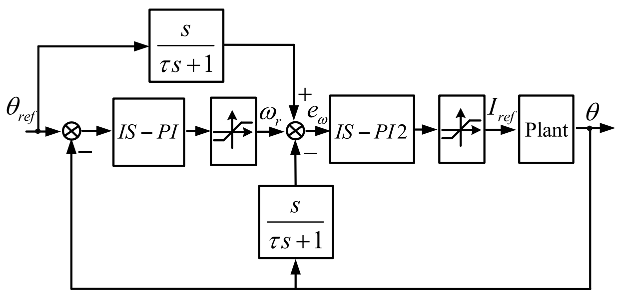

FIGURE 17. Block diagram of the IS-PI control.

In the experiment, Integral separation proportional integral (IS-PI) controller and Tanh controller are tested respectively. The block diagrams of the IS-PI and Tanh controller are shown in Fig.17 and Fig.18. In order to reduce the tracking error, speed feedforward is added. The parameters of IS-PI are $k_p = 110$, $k_i = 0.001$, $c = 60.45$, $e_0 = 0.05°$. The parameters of IS-PI2 are $k_p = 0.175$, $k_i = 0.05$, $c = 0$, and other parameters are $\omega_{\max} = 110$, $I_{\max} = 4A$, $\tau = 0.000796$. The parameters of tanh are $\omega_{\max} = 110$, $k_\omega = 1$.

B. EXPERIMENT RESULTS

1) A COMPARISON OF SINUSOIDAL SIGNAL TRACKING TEST

In this experiment, the reference signal is $\theta_{ref} = 5° + 5° \sin(\pi t)$, the maximum speed of tracking signal is $15.7°/s$,

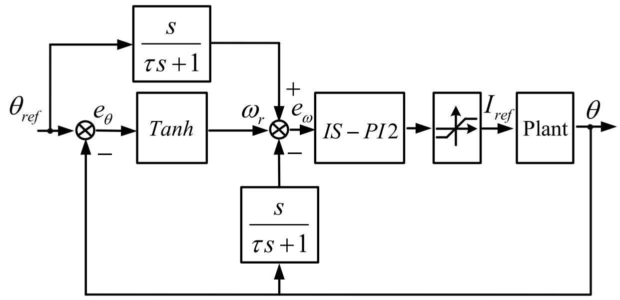

FIGURE 18. Block diagram of the Tanh control.

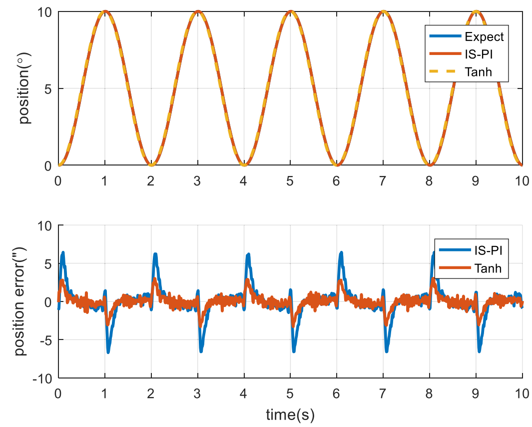

FIGURE 19. Sine signal $\theta_{ref} = 5° + 5° \sin(\pi t)$ tracking test.

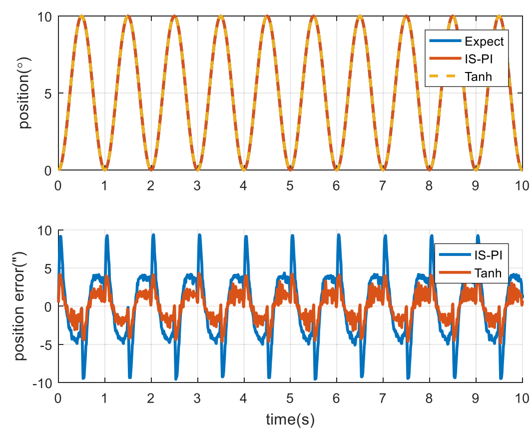

FIGURE 20. Sine signal $\theta_{ref} = 5° + 5° \sin(2\pi t)$ tracking test.

the results are shown in Fig.19 and table 3. The reference signal is $\theta_{ref} = 5° + 5° \sin(2\pi t)$, the maximum speed of tracking signal is $31.4°/s$, the results are shown in Fig. 20 and table 3.

From the sinusoidal signal tracking results, it can be seen that the proposed method in this paper effectively reduces the tracking error RMS (root mean square) value compared with the IS-PI controller, and the tracking error PV (peak-to-peak) value is greatly reduced. The position errors have a sinusoidal shape. That's because the closed-loop bandwidth of the control system cannot be very high, and there are steady-state

TABLE 3. Position error comparision.

Tracking signal	Control method position tracking error			
	IS-PI		Tanh	
	PV	RMS	PV	RMS
$5^\circ + 5^\circ \sin(\pi t)$	$13.25''$	$1.97''$	$6.63''$	$0.93''$
$5^\circ + 5^\circ \sin(2\pi t)$	$18.93''$	$4.37''$	$9.26''$	$1.94''$

PV stands for peak to peak value, RMS stands for root mean square. The unit is arc-second.

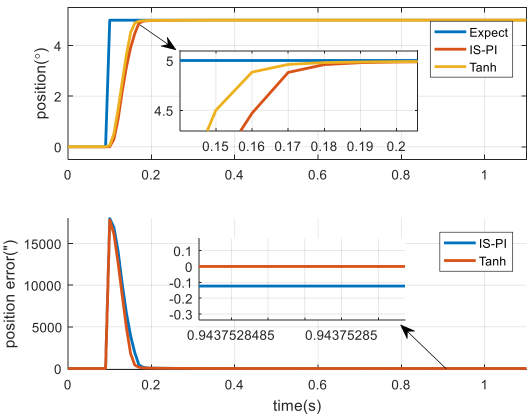

FIGURE 21. Step signal $0^\circ to 5^\circ$ tracking test.

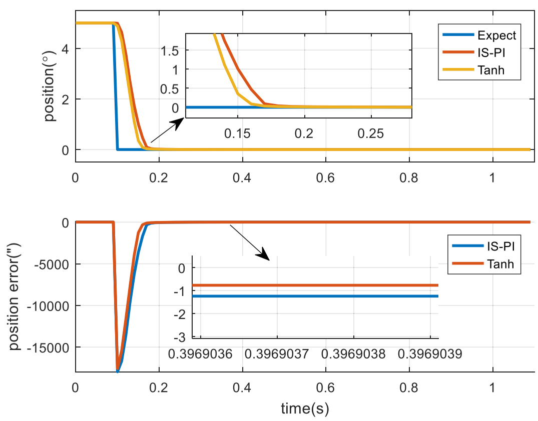

FIGURE 22. Step signal $5^\circ to 0^\circ$ tracking test.

errors when tracking a relatively higher frequency signal. The peaks in the position errors are caused by the change direction of the friction torque. When tracking reference signal is $\theta_{ref} = 5^\circ + 5^\circ \sin(\pi t)$, compared to IS-PI controllers, the tracking error RMS value is reduced by 53% and the PV value is reduced by 50%. When tracking reference signal is $\theta_{ref} = 5^\circ + 5^\circ \sin(2\pi t)$, compared to IS-PI controllers, the tracking error RMS value is reduced by 56% and the PV value is reduced by 51%.

2) A COMPARISON OF STEP SIGNAL TRACKING TEST

Step signal tracking results are shown in Fig. 21, Fig. 22, Fig. 23, Fig. 24, and table 4.

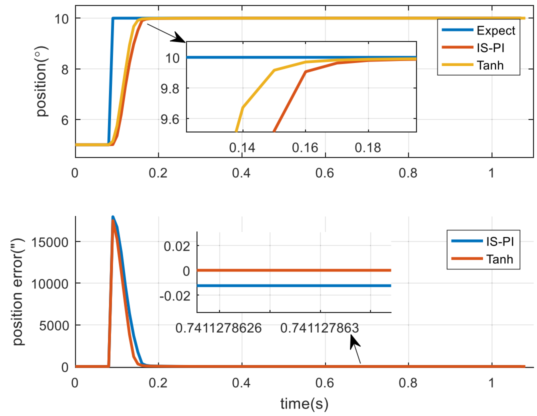

FIGURE 23. Step signal $5^\circ to 10^\circ$ tracking test.

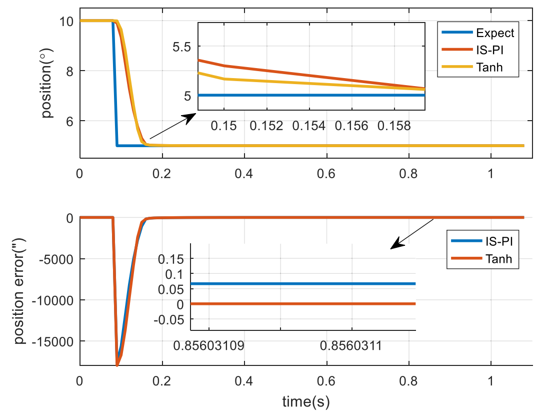

FIGURE 24. Step signal $10^\circ to 5^\circ$ tracking test.

TABLE 4. Position error comparision.

Tracking signal	Control method position tracking error	
	IS-PI	Tanh
$0^\circ to 5^\circ$	$0.78''$	$0.58''$
$5^\circ to 0^\circ$	$0.79''$	$0.57''$
$5^\circ to 10^\circ$	$0.92''$	$0.68''$
$10^\circ to 5^\circ$	$0.84''$	$0.74''$

PV stands for peak to peak value, RMS stands for root mean square. The unit is arc-second.

We can see that the tanh controller has smaller steady-state error, and faster response performance than IS-PI controller.It can be concluded that, by using the tanh controller, when tracking the step signal, the steady-state error is reduced by 12%.

3) A COMPARISON OF STEP SIGNAL TRACKING TEST WITH DISTURBANCE

The brake is used to act as external step disturbance, we add disturbance torque by controlling the brake, the test results are shown in Fig.25.

From the experiment results, we can see that the tanh method has the smaller tracking error compared with IS-PI method. Compared to the IS-PI method, the Tanh

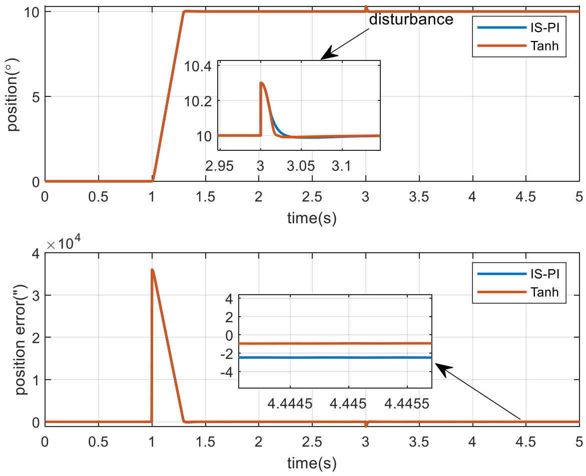

FIGURE 25. Step signal 0°*to*10° tracking test with disturbance.

TABLE 5. Turning parameters number of two method.

Method	Turning parameters number
IS-PI	3
Tanh	1

method has higher positioning accuracy, which is beneficial for improving the pointing accuracy of optical telescopes.

In addition, as shown in Table 5, the Tanh method only needs to adjust one parameter, which is easier to turning parameters than the IS-PI method.

V. CONCLUSION

This paper proposed a tanh algorithm to improve the control performance in the third mirror Z axis for a large optical telescope. Different from the traditional three closed-loop IS-PI control methods, a tanh algorithm is used in the position loop. The simulation and experiment results show that the proposed algorithm can improve both tracking accuracy and response performance. Compared to IS-PI controllers, Tanh controllers have a faster response and smaller steady-state error when tracking step signals. At the same time, the Tanh controller effectively reduces PV error value and RMS error value when tracking sinusoidal signals. There is only one parameter need to be turned in this method, and the parameter has clear physical significance, which can be calculated according to the control requirements, which is more convenient for use in engineering. In the further study, tanh control method can be extended to speed loop and current loop, a disturbance observer can be added to compensate for the disturbance caused by friction.

REFERENCES

[1] *Telescope Pointing*. [Online]. Available: http://www.tpointsw.uk/pointing.html

[2] U. Mutilba, G. Kortaberria, F. Egana, and J. A. Yagüe-Fabrae, "Relative pointing error verification of the telescope Mount assembly subsystem for the large synoptic survey telescope," in *Proc. 5th IEEE Int. Workshop Metrol. Aerosp. (MetroAeroSpace)*, Jun. 2018, pp. 155–160.

[3] Z. Sun, G. Wei, and G. Wang, "Optical pointing systems for the TM VGOS telescope," in *Proc. 13th Int. Conf. Commun. Softw. Netw. (ICCSN)*, Jun. 2021, pp. 314–317, doi: 10.1109/ICCSN52437.2021.9463612.

[4] X. He and X. Jiang, "Design and analysis of Lijiang 2.4-meter telescope Nasmyth focus and Cassgrain focus switching system," *Infr. Laser Eng.*, vol. 51, no. 5, pp. 374–382, May 2022, doi: 10.3788/irla20210881.

[5] W. Gawronski, "Control and pointing challenges of large antennas and telescopes," *IEEE Trans. Control Syst. Technol.*, vol. 15, no. 2, pp. 276–289, Mar. 2007, doi: 10.1109/TCST.2006.886434.

[6] J. Han, "From PID to active disturbance rejection control," *IEEE Trans. Ind. Electron.*, vol. 56, no. 3, pp. 900–906, Mar. 2009, doi: 10.1109/TIE.2008.2011621.

[7] X. Li, W. Zhou, J. Luo, J. Qian, W. Ma, P. Jiang, and Y. Fan, "A new mechanical resonance suppression method for large optical telescope by using nonlinear active disturbance rejection control," *IEEE Access*, vol. 7, pp. 94400–94414, 2019, doi: 10.1109/ACCESS.2019.2928050.

[8] C. Liu, G. Luo, X. Duan, Z. Chen, Z. Zhang, and C. Qiu, "Adaptive LADRC-based disturbance rejection method for electromechanical servo system," *IEEE Trans. Ind. Appl.*, vol. 56, no. 1, pp. 876–889, Jan. 2020, doi: 10.1109/TIA.2019.2955664.

[9] Y.-L. Zhang, M. Zhu, D. Li, and J.-M. Wang, "ADRC dynamic stabilization of an unstable heat equation," *IEEE Trans. Autom. Control*, vol. 65, no. 10, pp. 4424–4429, Oct. 2020, doi: 10.1109/TAC.2019.2957690.

[10] S. Yao, G. Gao, Z. Gao, and S. Li, "Active disturbance rejection synchronization control for parallel electro-coating conveyor," *ISA Trans.*, vol. 101, pp. 327–334, Jun. 2020, doi: 10.1016/j.isatra.2020.01.035.

[11] X. Li, W. Zhou, D. Jia, J. Qian, J. Luo, P. Jiang, and W. Ma, "A decoupling synchronous control method of two motors for large optical telescope," *IEEE Trans. Ind. Electron.*, vol. 69, no. 12, pp. 13405–13416, Dec. 2022, doi: 10.1109/TIE.2022.3142407.

[12] T. Samad, "A survey on industry impact and challenges thereof [technical activities]," *IEEE Control Syst. Mag.*, vol. 37, no. 1, pp. 17–18, Feb. 2017, doi: 10.1109/MCS.2016.2621438.

[13] R. P. Borase, D. K. Maghade, S. Y. Sondkar, and S. N. Pawar, "A review of PID control, tuning methods and applications," *Int. J. Dyn. Control*, vol. 9, no. 2, pp. 818–827, Jun. 2021, doi: 10.1007/s40435-020-00665-4.

[14] O. A. Somefun, K. Akingbade, and F. Dahunsi, "The dilemma of PID tuning," *Annu. Rev. Control*, vol. 52, pp. 65–74, May 2021, doi: 10.1016/j.arcontrol.2021.05.002.

[15] N. P. Lawrence, M. G. Forbes, P. D. Loewen, D. G. McClement, J. U. Backström, and R. B. Gopaluni, "Deep reinforcement learning with shallow controllers: An experimental application to PID tuning," *Control Eng. Pract.*, vol. 121, Apr. 2022, Art. no. 105046, doi: 10.1016/j.conengprac.2021.105046.

[16] O. Dogru, K. Velswamy, F. Ibrahim, Y. Wu, A. S. Sundaramoorthy, B. Huang, S. Xu, M. Nixon, and N. Bell, "Reinforcement learning approach to autonomous PID tuning," *Comput. Chem. Eng.*, vol. 161, May 2022, Art. no. 107760, doi: 10.1016/j.compchemeng.2022.107760.

[17] C. Tian-You, Z. Zheng, Z. Rui, L. Ning, and J. Yao, "PID tuning intelligent system based on end-edge-cloud collaboration," *ACTA Autom. Sinica*, vol. 49, no. 3, pp. 514–526, Mar. 2023, doi: 10.16383/j.aas.c230055.

[18] M. Chandra, "A novel method for scalable VLSI implementation of hyperbolic tangent function," *IEEE Des. Test.*, vol. 39, no. 1, pp. 85–91, Feb. 2022, doi: 10.1109/MDAT.2021.3063308.

[19] Z. Hajduk and G. R. Dec, "Very high accuracy hyperbolic tangent function implementation in FPGAs," *IEEE Access*, vol. 11, pp. 23701–23713, 2023, doi: 10.1109/ACCESS.2023.3253668.

[20] Y. Xiao, S. Chen, Q. Zhang, D. Lin, M. Shen, J. Qian, and S. Wang, "Generalized hyperbolic tangent based random Fourier conjugate gradient filter for nonlinear active noise control," *IEEE/ACM Trans. Audio, Speech, Language Process.*, vol. 31, pp. 619–632, 2023, doi: 10.1109/TASLP.2022.3230545.

[21] H. Zhang, "Modeling and control based on fuzzy hyperbolic model," *Acta Automatica Sinica*, vol. 26, no. 6, pp. 729–735, Jun. 2000, doi: 2000.10.1007/BF02950406.

[22] H. Zhang, J. Zhang, G.-H. Yang, and Y. Luo, "Leader-based optimal coordination control for the consensus problem of multiagent differential games via fuzzy adaptive dynamic programming," *IEEE Trans. Fuzzy Syst.*, vol. 23, no. 1, pp. 152–163, Feb. 2015, doi: 10.1109/TFUZZ.2014.2310238.

[23] Z. Huaguang and Q. Yongbing, "Modeling, identification, and control of a class of nonlinear systems," *IEEE Trans. Fuzzy Syst.*, vol. 9, no. 2, pp. 349–354, Apr. 2001, doi: 10.1109/91.919256.

[24] L. Liu, Z. Wang, Z. Huang, and H. Zhang, "Adaptive predefined performance control for MIMO systems with unknown direction via generalized fuzzy hyperbolic model," *IEEE Trans. Fuzzy Syst.*, vol. 25, no. 3, pp. 527–542, Jun. 2017, doi: 10.1109/TFUZZ.2016.2566803.

[25] A. K. Peter, J. Mathew, and K. Gopakumar, "A simplified DTC-SVPWM scheme for induction motor drives using a single PI controller," *IEEE Trans. Power Electron.*, vol. 38, no. 1, pp. 750–761, Jan. 2023, doi: 10.1109/TPEL.2022.3197362.

[26] Y. Fan, J. Chen, Q. Zhang, and M. Cheng, "An improved inertia disturbance suppression method for PMSM based on disturbance observer and two-degree-of-freedom PI controller," *IEEE Trans. Power Electron.*, vol. 38, no. 3, pp. 3590–3599, Mar. 2023, doi: 10.1109/TPEL.2022.3218842.

[27] P. Schipani, C. Arcidiacono, J. Argomedo, M. Dall'Ora, S. D'Orsi, J. Farinato, D. Magrin, L. Marty, R. Ragazzoni, and G. Umbriaco, "The tracking control system of the VLT survey telescope," *Rev. Sci. Instrum.*, vol. 83, no. 9, Sep. 2012, Art. no. 094501, doi: 10.1063/1.4754128.

[28] A. M. Cohen, *Numerical Methods for Laplace Transform Inversion*. Cham, Switzerland: Springer, 2007.

[29] B. Davies and B. Martin, "Numerical inversion of the Laplace transform: A survey and comparison of methods," *J. Comput. Phys.*, vol. 33, no. 1, pp. 1–32, Oct. 1979.

[30] T. Blickle, "The hyperbolic tangent distribution family," *Powder Technol.*, vol. 97, pp. 100–108, Jun. 1998.

[31] N. Batir, "On some properties of digamma and polygamma functions," *J. Math. Anal. Appl.*, vol. 328, no. 1, pp. 452–465, Apr. 2007.

WENLIN ZHOU received the B.S. and M.S. degrees from the School of Automation, Northwestern Polytechnical University, China, in 2012 and 2015, respectively. She is currently a Research Associate with the Institute of Optics and Electronics (IOE), Chinese Academy of Sciences (CAS), China. Her research interests include robust control, ADRC, PMSM, and motion control systems.

KUN XIE received the Ph.D. degree in optical engineering from the National University of Defense Technology. He is currently an Engineer with the Xi'an Satellite Control Center, Xi'an, China. His research interests include adaptive optics, fiber lasers, and large photoelectric telescopes.

JUNZHANG QIAN received the B.S. degree from the School of Automation, Northwestern Polytechnical University, China, in 2012, and the Ph.D. degree from the Institute of Optics and Electronics (IOE), Chinese Academy of Sciences (CAS), China, in 2017. He is currently a Research Associate with IOE, CAS. His research interests include PMSM, sliding mode control (SMC), and robust control.

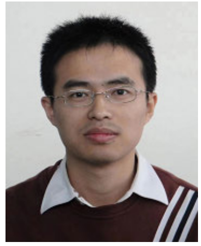

MO XIA received the B.S. degree from Wuhan University, Wuhan, China, and the M.S. degree from the University of Science and Technology of China, China. He is currently an Associate Researcher with the Institute of Optics and Electronics (IOE), Chinese Academy of Sciences (CAS), China. His research interests include photoelectric detection, automation control, and large photoelectric telescopes.

YI PU received the B.S. degree from Sichuan Normal University, Chengdu, China, and the M.S. degree from the University of Science and Technology of China, China. He is currently an Associate Researcher and a Master's Supervisor with the Institute of Optics and Electronics (IOE), Chinese Academy of Sciences (CAS), China. His main research interests include the overall technology of photoelectric telescopes, the overall design of automation control, and system integration.

JINLONG HUANG received the Ph.D. degree from the University of Electronic Science and Technology of China. He is currently a Research Fellow with the Institute of Optics and Electronics (IOE), Chinese Academy of Sciences (CAS), China. His research interests include photoelectric detection, precision machinery, and large photoelectric telescopes.

XIN LI received the B.S. and M.S. degrees from the School of Automation, Northwestern Polytechnical University, China, in 2011 and 2014, respectively, and the Ph.D. degree from the Institute of Optics and Electronics (IOE), Chinese Academy of Sciences (CAS), China, in 2020. His research interests include robust control, ADRC, and high-precision servo control systems in large photoelectric telescopes.